The Effects of Geometry and Substrate Material on Thermoelectric Generator Performance

Xi Wang, David S.-K. Ting, and Paul Henshaw[✉]

Turbulence and Energy Laboratory, University of Windsor,
401 Sunset Avenue, Windsor, ON, Canada
`henshaw@uwindsor.ca`

Abstract. As a solid-state energy convertor, the thermoelectric generator (TEG) has been widely applied in heat recovery systems. However, its lower efficiency (about 5–7%) is one of the main challenges to employ the TEG technology further. Based on simulations, this research mainly investigated the effects of geometry parameters and substrate materials on TEG performance. A 3-D model for a TEG was created using ANSYS Workbench and validated using experimental results from the literature. A dimensionless parameter, shape factor ratio, was used to describe the geometrical characteristics of the P-N couples. In this study, this parameter is actually a ratio between the cross-sectional area of P and N semiconductors. Five values of shape factor ratios were considered. In addition, various combinations of couples' lengths were also simulated as it is an important geometric parameter of a TEG. Finally, the effect of the substrate material (Zirconia, Boron Nitride, Aluminum Oxide, Aluminum Nitride, and Silicon Carbide) on the TEG performance was analyzed. Through the modeling study, it was shown that the performance of this TEG model is maximized when the shape factor ratio is 1. Meanwhile, couple length had opposite effects on output power and efficiency of the TEG. Finally, it was found that the most conductive substrate (Silicon Carbide) resulted in the best TEG performance.

1 Introduction

It is well-known that thermal engines produce a large amount of waste heat [1]. For instance, about 70% of energy is wasted into the cooling system and exhausted gases by an automobile engine [2]. Likewise, around 30% of the energy is wasted in the same way by furnaces and boilers [3]. Therefore, it is worthwhile to develop thermal recovery technology to reuse waste heat, making it possible to conserve more energy.

The development of TEG systems is an effort to recover the waste heat [4]. The core component of a TEG system is the TEG module, a semiconductor-based energy converter [5]. It is always sandwiched between a heat source and a radiator [6]. This energy conversion system is mainly based on the thermoelectric effects, especially Seebeck and Peltier effects, *i.e.*, utilizing temperature difference to produce electricity [7–9]. Recently, TEG systems have been applied in some industrial fields, *i.e.* automobiles and solar power systems [2, 10, 11]. However, the low efficiency of TEG modules (about 5%) is considered as one of the outstanding challenges impeding this technology from further development [12].

According to the theories of TEG, its efficiency depends on the TEG module structure and materials [3]. A TEG module consists of substrates, conductors and TE couples. The substrate is the exterior pathway for heat absorption or dissipation. The TE couple is the core component to conduct thermoelectric conversion. Thus, the optimization of the structure mainly focusses on the filling fraction (ratio of total TE couple area and substrate area), the geometric dimensions of the TE couple and shape of the TE couple. Some studies on this aspect have been done in recent years. Using a 1-D TEG model, the results from Meng *et al.* indicated that the efficiency of the TEG with 60% filling fraction is better than that of other values of filling fraction [13]. Based on a 3-D TEG model, Karri and Mo tested the influence of different cross-sectional shapes on a TEG's reliability [14]. The results indicated that shapes without sharp corners (like a round cross-sectional area) have a better reliability due to their lower stress concentrations under the same temperature condition [14]. Likewise, Wang et al. used a 3-D model to compare two types of TEG shape: R-TEG with a round cross-sectional area, and C-TEG with a square cross-sectional area [15]. They found that the output power of R-TEG was higher than that of C-TEG; however, they observed an inverse result in efficiency [15]. In addition to the structure of the TEG module, materials also play a dominant role in a TEG's performance. TE materials have developed at an astounding pace over the past decades, especially the application of nano-materials and superlattice materials. The efficiency of some TEGs has even reached at 20% [12, 16–19]. Some substrate materials have direct impacts on heat absorption and dissipation. In 2012, Rezania and Rosendhl utilized ANSYS-Workbench to analyze the effects of using different ceramic materials as substrates on the heat distribution in a TEG [20].

Through modelling studies, some researchers have considered different semiconductor shapes with various roundness and number of sides. A dimensionless parameter, named shape factor ratio (D), was used to describe the geometric characteristics of the TE couple, making it possible to compare studies [21]. The TE couple consists of a P semiconductor and an N semiconductor. Hence, D is defined as the ratio between the cross-sectional area of the two kinds of semiconductors for each TE couple. Based on the TEG theory, the TE couple length (distance parallel to heat flow) is considered as a significant factor in TEG performance. However, it is also necessary to make clear the relationship between the couple length and TEG performance. Additionally, heat is absorbed and dissipated via the substrate. The thermal conductivity of substrate materials decides how much heat can be converted to electricity by the TE couples. On the other hand, a higher electrical conductivity leads to short-circuiting. Therefore, one should not lose sight of the important influence of substrate materials on TEG performance.

This paper mainly focuses on the effects of shape factor, TE couple length and substrate material on TEG performance through a 3-D TEG model. In this way, a TEG model was created through ANSYS Workbench and validated using the experimental results of Hsu et al. [22]. The open circuit voltage, current, output power, and efficiency are important output characteristics, and were used to evaluate the TEG performance in this study. Upon validation, the modelling study analyzed the influences of shape factors and TE couple length on the TEG output characteristics. Moreover, in order to determine a relationship between substrate materials and TEG performance, the present

study considered five common ceramic materials: Zirconia, Boron Nitride, Aluminum Oxide, Aluminum Nitride and Silicon Carbide.

2 Performance Characteristics of a TEG

A TEG module normally consists of three main parts: the TE couple, the conductor and the substrate (as shown in Fig. 1) [20]. Each TE couple consists of a pair of semiconductors (P material and N material), connected by an electrically conductive material, such as copper or aluminum. Finally, the module is packaged on a substrate, which is an electrically insulating material, such as Al_2O_3 ceramic or SiO_2 [21–24].
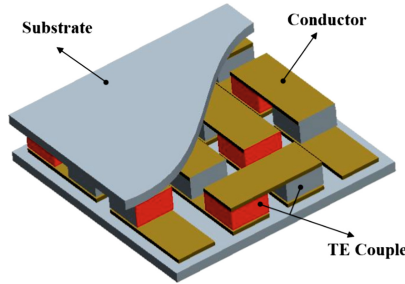
Fig. 1. Structural diagram of a TEG module

A TEG module can create electricity when having a temperature difference on both sides of the module. According to the Seebeck effect and Ohm's law, the output power can be calculated by the Eq. (1) [17]:

$$P = I^2 r_L = \frac{S^2(T_h - T_c)^2 r_L}{(r_i + r_L)^2} \tag{1}$$

where, I is current; r_L and r_i are load resistance and internal resistance; S is Seebeck coefficient; T_h and T_c are the temperatures of hot and cold side.

When load resistance equals internal resistance, the output power of a TEG module will reach a maximum value [17].

$$P_{max} = \frac{S^2(T_h - T_c)^2}{4r_i} \tag{2}$$

In order to calculate the efficiency of a TEG module, it is necessary to analyze the thermal transfer process (as shown in Fig. 2(a)). The thermal energy flows through a TEG system to produce electrical power. However, according to the second law of thermodynamics [1], it is inevitable to lose some thermal energy doing work. Therefore, some input energy will be lost through Fourier heat and Peltier heat.

Due to internal resistance, Joule heat will be created in the TEG module when current flows through a TE couple. In this paper, it was assumed that the edge of the TE couple is adiabatic. In this way, it was assumed that the Joule heat can be transferred to both

ends of the TE couple when current comes through it. In this way, it was assumed that the heat source absorbs a half of Joule heat and the other half dissipates into the heat sink (shown in Fig. 2(a)) [3, 21].

When analyzing the energy balance for the hot side, there are two kinds of energy absorbed by the hot side substrate: input heat and Joule heat. The hot side absorbs only half of the Joule heat, for the other half is absorbed by the cold side. Meanwhile, there are two kinds of energy coming out of the hot side, which are Fourier heat and Peltier heat (shown by Fig. 2(a)). In this way, at steady-state, the heat input rate is [21, 25]:

$$\dot{Q}_{input} = \dot{Q}_F + \dot{Q}_P - \frac{1}{2}\dot{Q}_J \tag{3}$$

Therefore, the efficiency of a TEG module can be defined as Eq. (4) [21, 25]:
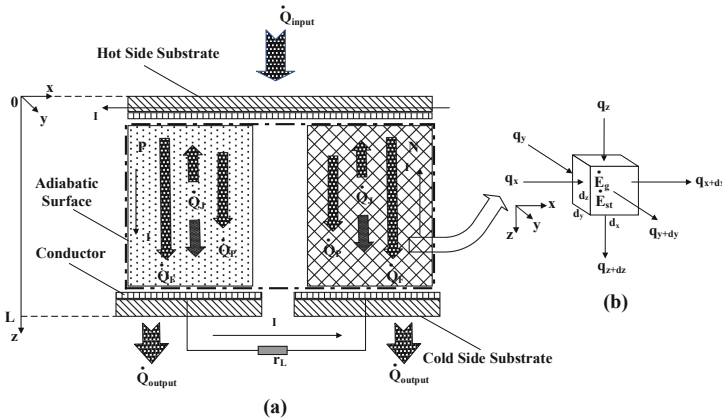
$$\eta = \frac{P}{\dot{Q}_{input}} = \frac{\frac{S^2(T_h-T_c)^2 r_L}{(r_i+r_L)^2}}{\dot{Q}_F + \dot{Q}_P - \frac{1}{2}\dot{Q}_J}$$

$$= \frac{\frac{S^2(T_h-T_c)^2 r_L}{(r_i+r_L)^2}}{k(T_h - T_c) + ST_h \frac{S(T_h-T_c)}{r_i+r_L} - \frac{1}{2}[\frac{S(T_h-T_c)}{r_i+r_L}]^2 r_i} \tag{4}$$

in which k is the thermal conductivity of a TE couple.

In order to simplify the efficiency equation, two parameters were introduced, which are the ratio of the load resistance and internal resistance (m) and the thermoelectric figure of merit (Z).

$$m = \frac{r_L}{r_i} \tag{5}$$

$$Z = \frac{S^2}{kr_i} \tag{6}$$

Fig. 2. Schematic diagram of a TEG heat transfer process (a) in the entire TEG module, and (b) in a control volume using Cartesian coordinates

Therefore, the efficiency can be calculated by Eq. (7)

$$\eta = \frac{T_h - T_c}{T_h} \frac{\frac{m}{m+1}}{\left(1 + \frac{m+1}{ZT_h} - \frac{1}{2}\frac{T_h - T_c}{T_h}\frac{1}{m+1}\right)} \tag{7}$$

3 Numerical Model of a TEG

In this paper, a 3-D numerical model was used to analyze the performance of a TEG. Hence, a series of governing equations was built to describe the working process of the TEG. In order to acquire the numerical results, the TEG model needs to conduct discrete transformation, meanwhile, using reasonable boundary conditions.

3.1 Governing Equations for TEG Model

Based on ANSYS-Workbench, a steady-state TEG model was developed. For each control volume, the governing equations were established based on energy balance and electric charge continuity. According to an energy balance (shown by Fig. 2(b)), the energy storage term equals the sum of the net energy flow into and energy generation in a control volume [26–28]:

$$E_{st} = E_{in} - E_{out} + E_g \tag{8}$$

where E_{st} is the energy storage term, which can be calculated by Eq. (9). However, this simulation is steady-state, so the E_{st} is 0. In addition, E_{in} is total energy input. From Fig. 1(b), E_{in} is the sum of energy input from three directions (Eq. (10)). Similarity, the total energy output (E_{out}) is sum of energy output from three directions (Eq. (11)). Finally, E_g is the energy generation in the control volume, which is Joule heat (calculated by Eq. (12)) [26–28].

$$E_{st} = \rho c_p \frac{\partial T}{\partial t} dx\, dy\, dz = 0 \tag{9}$$

$$E_{in} = q_x\, \mathrm{dy\, dz} + q_y\, \mathrm{dx\, dz} + q_z\, \mathrm{dx\, dy} \tag{10}$$

$$E_{out} = \left(q_x + \frac{\partial q_x}{\partial x}dx\right)\mathrm{dy\, dz}$$
$$+ \left(q_y + \frac{\partial q_y}{\partial y}dy\right)\mathrm{dx\, dz}$$
$$+ \left(q_z + \frac{\partial q_z}{\partial z}dz\right)\mathrm{dx}\, dy \tag{11}$$

$$E_g = \left([\rho]\vec{j} \cdot \vec{j}\right)dx\, dy\, dz \tag{12}$$

in which q_x, q_y and q_z are heat fluxes in three directions; $\vec{j}$ is the current density vector.

The energy balance for the control volume can be represented by Eq. (13). The left term of Eq. (13) represents divergence of the heat flux vector (shown in Eq. (14)). Meanwhile, based on the theory of TEG, the heat flux vector for a control volume mainly consists of Fourier heat flux and Peltier heat flux. Thus, the energy for a control volume is the vector sum of Fourier heat flux and Peltier heat flux (shown in Eq. (15)) [26–28].

$$\frac{\partial q_x}{\partial x} + \frac{\partial q_y}{\partial y} + \frac{\partial q_z}{\partial z} = [\rho] \overrightarrow{j} \cdot \overrightarrow{j} \tag{13}$$

$$\nabla \cdot q = [\rho] \overrightarrow{j} \cdot \overrightarrow{j} \tag{14}$$

$$q = [S]T \cdot J - [k] \cdot \nabla T \tag{15}$$

In this way, the energy balance is described by Eq. (16), which is the integration of Eqs. (14) and (15).

$$\nabla \cdot ([S]T \cdot J - [k] \cdot \nabla T) = [\rho] \overrightarrow{j} \cdot \overrightarrow{j} \tag{16}$$

Additionally, the control volume must be consistent with electric charge continuity; namely, the amount of electric charge in any closed volume of space must be 0 under a constant electric field [26–28]. Thus, the electric charge continuity equation becomes:

$$\nabla \cdot J = 0 \tag{17}$$

Therefore, Eqs. (16) and (17) are governing equations for the TEG model. In these equations, S, k and ρ are the Seebeck coefficient matrix, thermal conductivity matrix and electric resistivity matrix (represented by Eqs. (18) to (20)) [26].

$$[S] = \begin{bmatrix} S_{xx} & & \\ & S_{yy} & \\ & & S_{zz} \end{bmatrix} \tag{18}$$

$$[k] = \begin{bmatrix} k_{xx} & & \\ & k_{yy} & \\ & & k_{zz} \end{bmatrix} \tag{19}$$

$$[\rho] = \begin{bmatrix} \rho_{xx} & & \\ & \rho_{yy} & \\ & & \rho_{zz} \end{bmatrix} \tag{20}$$

3.2 Boundary Conditions

In order to calculate the governing equation, it is necessary to add some boundary conditions. As for the thermal boundary, the first boundary condition was applied both on the cold and the hot side:

For the surface at $z = 0$;

$$T = T_h \tag{21}$$

For the surface at z = L;

$$T = T_c \tag{22}$$

As for the electrical boundary conditions, the load resistance was kept same as internal resistance. A surface of the TEG was settled as electric potential reference with 0 mV.

3.3 Numerical Solution

The TEG model described above needs to conduct discrete transformation during the numerical calculation. Normally, the discrete methods can be divided into three different types, which are finite difference method (FDM), finite element method (FEM), and finite volume method (FVM). In this paper, the modeling study of a TEG was done through ANSYS-Workbench software. In this way, the TEG model was discretized using FVM during the process of solution [28]. Namely, the TEG domain was divided into many control units by mesh, which can be connected by nodes. As for each node, it is equipped with a finite volume, making it possible to solve the differential governing equations through integration for each finite volume.

4 TEG Model Verification and Validation

This section describes a TEG modelled by ANSYS Workbench, and how model verification arrived at a reasonable mesh type and node numbers. After that, an experimental result reported by Hsu *et al.* [22] was used to validate the TEG model.

### 4.1 Establishment and Simplification of TEG Model

Based on Hsu *et al.*, a TEG model with 199 pairs of couples was established, as shown in Fig. 3. The initial dimension of the TEG was 60 mm × 60 mm × 2.91 mm. Inside, the initial dimension of the individual semiconductors and electric conductors were 2 mm × 2 mm × 0.64 mm and 4.5 mm × 2 mm × 0.5 mm, respectively.
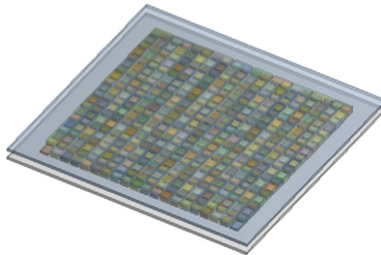
Fig. 3. TEG model geometrical structure (199 couples)

The TEG model consisted of 199 pairs of couples, being considered as 199 batteries in series. Hence, the total voltage is the sum of each couple's voltage. In this way, the

model was simplified as 2 pairs of couples. The simplified model can be seen in Fig. 4. Table 1 provides some information about material properties. Duo to similar absolute value of constant material properties, some similar equations were used to describe variable material properties in this paper.
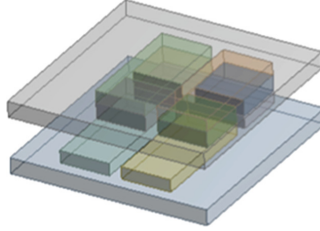
Fig. 4. Simplified TEG model structure (two couples)

Table 1. Material properties in the TEG model [22, 29]

Parameter	P semiconductor	N semiconductor	Copper	Ceramic
Seebeck coefficient (μVK^{-1})	Constant 215	Constant -212	–	–
	Variable $\pm (22224 + 930.6 \times T - 0.9905 \times T^2) \times 10^{-3}$			
Thermal conductivity ($Wm^{-1}K^{-1}$)	Constant 1.373	Constant 1.456	385	22
	Variable $(62605 - 277.7 \times T + 0.4131 \times T^2) \times 10^{-4}$			
Resistivity ($\mu\Omega m$)	Constant 1.04×10^4	Constant 1.04×10^4	3.2×10^{-8}	1×10^{12}
	Variable $51120 + 1634 \times T + 6.279 \times T^2$			
Contact area (mm^2)	4	4	9	9
Thickness (mm)	0.64	0.64	0.5	0.635

4.2 Model Verification

As is known, the simulation results may be affected by the coarseness of the grid. Therefore, it is necessary to have the best mesh type and acquire a grid-independent solution at the outset of the modeling study. During the process of the research, it was assumed that the contact thermal resistance and electric resistance could be ignored. Besides, the TE couple length is very small, and insulating material fills any space around the semi-conductors. Therefore, it is reasonable to assume adiabatic condition for the surrounding of TE couples. Meanwhile, the cold side was fixed at 573 K and the hot side was set to 603 K. In addition, the electric potential of a surface with 0 mV was set as a reference. The configuration is shown in Fig. 5.
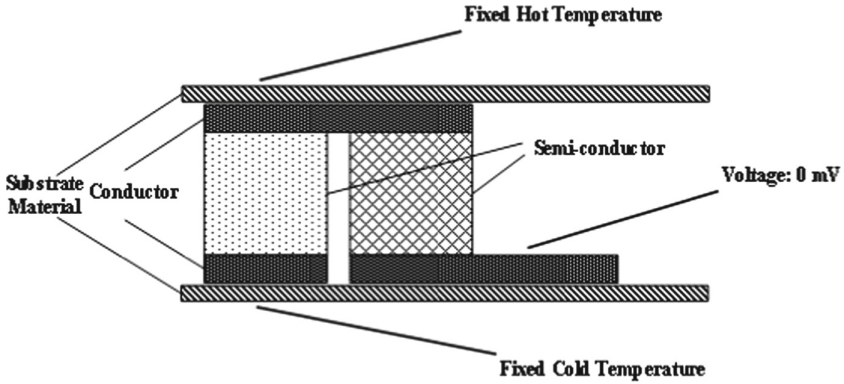
Fig. 5. Schematic cross-section of a PN couple showing boundary conditions

In order to ensure that the best mesh type, three kinds of meshes (Hex, Tet and Mix) were used in the model. The grid nodes numbered 3×10^5 in the three cases. The results are shown in Fig. 6, from which it is concluded that the difference of the open circuit voltage with the three kinds of meshes was just 0.06%. Thus, a Hex mesh was used in further studies, as it has the best average element quality (ratio of volume and side length of a mesh element) of 0.943 under the same computational conditions, compared with the two others.
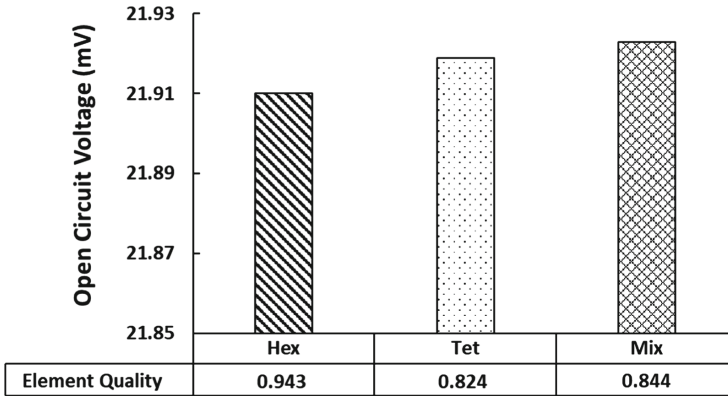

Fig. 6. Comparison of mesh type based on open circuit voltage

After determining the mesh type, it was desired to acquire a grid-independent solution. In this way, seven values of grid node number were considered in this study. According to the results (Fig. 7), the variation of open circuit voltage was almost negligible (the rate of change was about 0.01%) when the number of grid nodes reached more than 3×10^5. Thus, the modeling study used grid conditions in which the node number is about 3×10^5. These grid conditions ensured a relatively convergent result, saving computational resources.
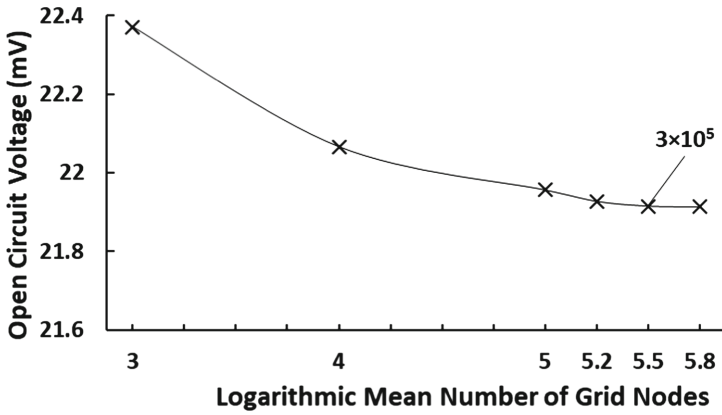
Fig. 7. Open circuit voltage with different logarithmic mean number of grid nodes

4.3 Model Validation

The validation of the TEG model was done before using it in further studies. In this paper, experimental data from Hsu *et al.* was used to check the simulation result [22]. Therefore, the temperature of the cold side was fixed at 573 K, and the temperature of the hot side was set from 578 to 613 K in the model. Then, the open circuit voltage from the model was compared with the Hsu group results.

In this work, there were three parameters used in the model that could be constant or variable (Table 1). According to the results (Fig. 8), there is a similar trend of open circuit voltage with temperature difference in the three cases: the voltage value had a linear increase with the temperature. Compared with the results of the experiment, the average error of the simulation results with constant properties (25.6%) is higher than that with variable properties (16.7%) when the temperature difference was 40 K. In order to make the TEG performance more meaningful, it was necessary to increase the temperature difference in further studies. Using a linear relationship between the experimental open
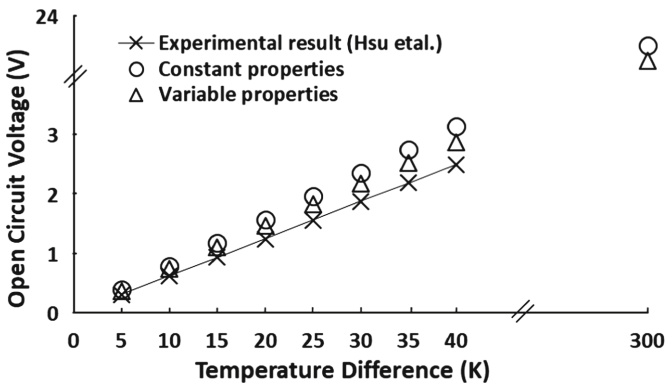

Fig. 8. Comparison of simulations with experimental results

circuit voltage and the temperature difference, and running the model at a temperature difference of 300 K, it was predicted that the average error of the simulation result with variable properties was 19.1%, which was again lower than that for constant properties (25.5%). Hence, the TEG model with variable properties was used for further studies.

5 The Effects of Geometric Structure and Substrate Material on TEG Performance

In this section, the validated TEG model was used to analyze the effects of the TEG geometrical structure on its performance. Additionally, the TEG with different substrate materials was also modelled in order to illustrate its influence on the TEG performance under the same working temperature condition.

5.1 The Effects of Shape Factor Ratios on TEG Performance

As is known, the thermoelectric figure of merit (Z) plays a dominant role in a TEG performance [16, 17]. Based on Eq. (6), Z is mainly decided by the Seekbeck coefficient (S), system conductivity (k) and internal resistance (r_i), where (k) and (r_i) can be calculated by the follow equations:

$$k = \frac{k_p A_p}{L_p} + \frac{k_n A_n}{L_n} \tag{23}$$

$$r_i = \frac{\rho_p L_p}{A_p} + \frac{\rho_n L_n}{A_n} \tag{24}$$

From these equations, the value of Z has a close relationship with the geometry of the P&N thermoelectric couple. Therefore, two parameters named shape factor (D_n, D_p) and shape factor ratio (D), were discussed in this paper. The shape factors are [21]:

$$D_p = \frac{L_p}{A_p} \tag{25}$$

$$D_n = \frac{L_n}{A_n} \tag{26}$$

The shape factor ratio is [21]:

$$D = \frac{D_p}{D_n} = \frac{L_p A_n}{L_n A_p} \tag{27}$$

where normally, $L_p = L_n$.

Therefore:

$$D = \frac{A_n}{A_p} \tag{28}$$

In order to make the research more meaningful, the maximal temperature difference was enlarged to 300 K. During this set of simulations, the temperature of the cold side was fixed at 303 K, and the temperature of the hot side was set from 373 K to 573 K. The value of m was 1, namely; the internal resistance equaled the load resistance. Also, the total cross-sectional area of both P and N semiconductors were kept the same at 8 mm^2. There were five values of shape factor ratios considered in this study, which were 0.25, 0.5, 1, 2 and 4. The output power and efficiency were calculated under each condition.

According to Fig. 9, at each specific T_h, the output power reached a maximum, when $D = 1$. That for $D = 0.5$ comes second in the graph, which has the same value as when D equals 2. However, the smallest output power was calculated for $D = 0.25$ and $D = 4$. It can be imagined for this study that the TEG module limits the current passing through the P&N couple to that passing through the material having the smallest cross-sectional area because it has the highest internal resistance. Hence, the current is maximized when the shape factor ratio is 1. At each specific value of D, the output power had an obvious increasing trend with the growth of T_h. The reason is that a higher temperature on the hot side means a larger temperature difference, making it possible to produce more current.
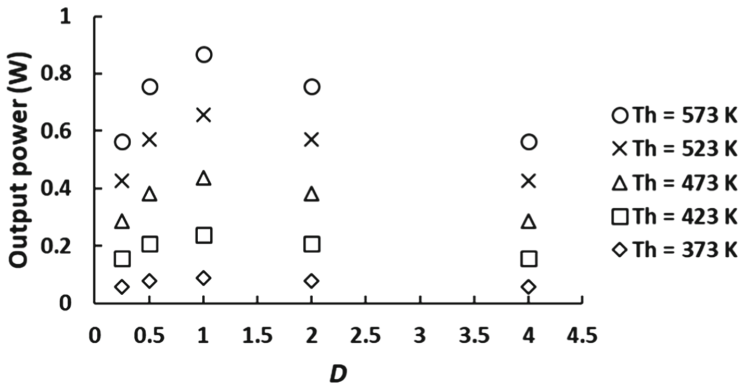

Fig. 9. Output power at different hot temperature and shape factor ratios

In addition, there are some similar tendencies that are shown in Fig. 10. However, the most obvious difference happened in the change of the efficiency with different T_h for a specific D. At lower T_h, there was an increase in the value of the efficiency with temperature. However, the change in efficiency became negligible at higher T_h. Although the output power of the TEG module increases with temperature of the hot side, the increase in T_h results in a higher input thermal energy. Therefore, based on the efficiency equation (Eq. (7)), the temperature of the hot side and the temperature difference have contradictory impacts on the TEG efficiency.

Though this study, it was found that the TEG performance was the best when $T_h = 573$ K and $D = 1$. All further simulations in this paper used these same conditions.
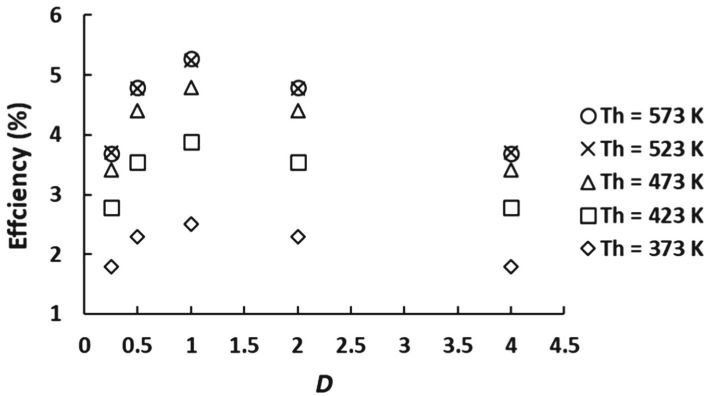
Fig. 10. Efficiency at different hot temperature and shape factor ratios

5.2 The Effects of Couple Length on TEG Performance

According to the theory of operation of this TEG, its performance has a close relationship with an internal resistance, working temperature and thermoelectric materials. Equation (24) illustrates that the couple length (L) has an important influence on this parameter. Therefore, in order to illustrate this effects, seven values of couple lengths were used in this modeling study: 0.32 mm, 0.48 mm, 0.64 mm, 0.8 mm, 0.96 mm, 1.12 mm, and 1.28 mm. Meanwhile, other computational conditions and geometry properties were kept the same. For evaluation, some parameters relative to the TEG performance were calculated: internal resistance, output power, and efficiency.

There was a totally different variation in the output power and efficiency as couple length was varied. Figure 11 shows that the output power decreased modestly from 1.38 W at 0.32 mm to 0.49 W at 1.28 mm. However, there was a moderate increase in the TEG efficiency, from 4.87% to 5.53%, over the same range. Additionally, Fig. 12 shows the variation of the internal resistance with couple length. The internal resistance experienced a dramatic growth with the couple length increase, from 0.0076 Ω at 0.32 mm
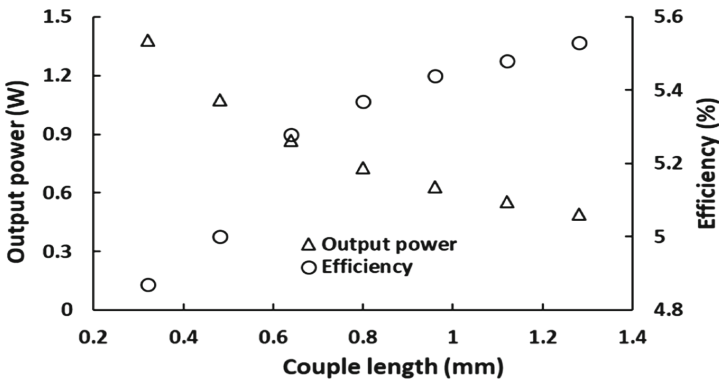

Fig. 11. Output power and efficiency at different couple lengths

to 0.0293 Ω at 1.28 mm. Obviously, the increase of internal resistance can weaken the current, leading to a lower output power and Peltier heat. Besides, the Peltier heat is also a part of the input thermal energy. Therefore, the rise of the internal resistance is one of the main reasons why the efficiency and output power change in different ways.
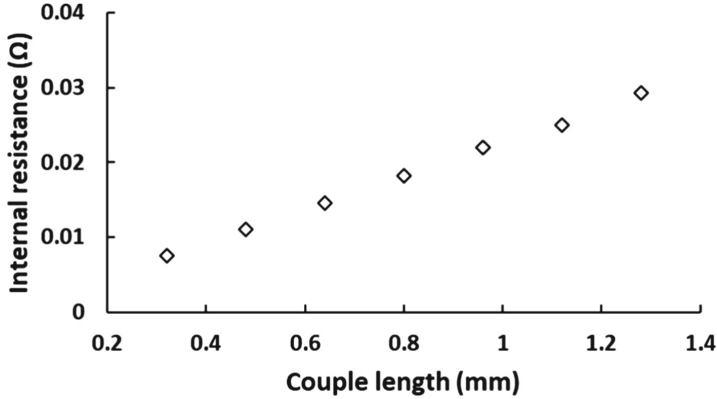

Fig. 12. Internal resistance at different couple lengths

5.3 The Effects of Substrate Material on TEG Performance

As was stated in Sect. 2, a TEG module consists of three main parts: the substrates, conductors and thermoelectric couple [20]. Therefore, the thermal energy must diffuse through the three parts successively when the TEG is working. Based on the Fourier theory, the thermal conductivity of the substrate material has an influence on the thermal energy diffusion process, making it possible to affect TEG performance. In this paper, five kinds of substrate materials were simulated: Zirconia, Boron Nitride, Aluminum Oxide, Aluminum Nitride, and Silicon Carbide. The thermal conductivities of the materials are shown in Table 2. Meanwhile, other computational conditions and geometric properties were kept the same, while calculating the output power, efficiency and current.

Table 2. Thermal conductivity of substrate materials [20, 30]

Substrate material	Zirconia	Boron Nitride	Aluminum Oxide	Aluminum Nitride	Silicon Carbide
Thermal conductivity $(Wm^{-1}K^{-1})$	2.2	15	22	100	150

According to Fig. 13, both the output power and efficiency experienced a dramatic increase with a rise of the substrate material conductivity, which ranged from 0.240 W and 3.20% at 2.2 $Wm^{-1}K^{-1}$ to 1.05 W and 5.62% at 150 $Wm^{-1}K^{-1}$, respectively.

Unlike the effect of varying T_h alone (Fig. 10), in these simulations the temperature difference across the whole TEG was fixed at 270 K, so the denominator of Eq. (7) was constant. Hence, both the efficiency and output power increased. However, the change of the output power and efficiency leveled off when the substrate material conductivity exceeded 22 $Wm^{-1}K^{-1}$. In addition, a similar trend can be found in Fig. 14. The change of the current and open circuit voltage was from 4.07 A and 119 mV at 2.2 $Wm^{-1}K^{-1}$ to 8.49 A and 248 mV at 150 $Wm^{-1}K^{-1}$.
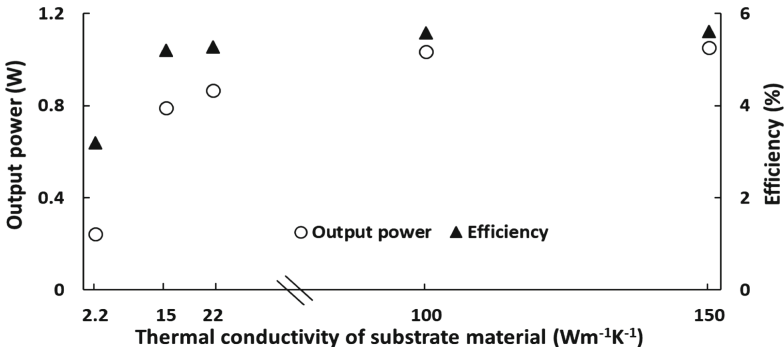

Fig. 13. Output power and efficiency with different substrate materials
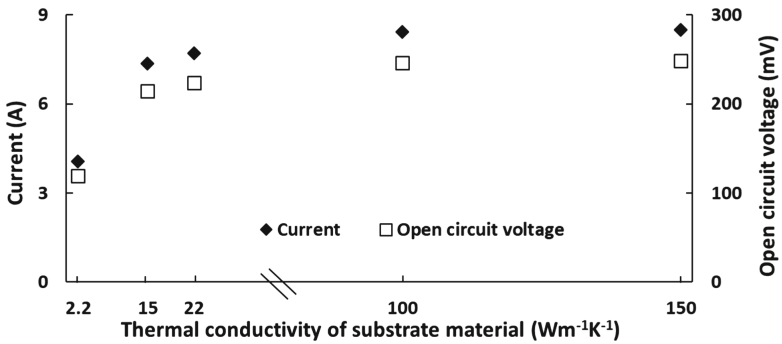

Fig. 14. Current and open circuit voltage with different substrate materials

Figure 15 shows the change of the maximum temperature gradient on the thermoelectric couple (as opposed to the whole TEG device) with different substrate material conductivities, which mimics the variation in the TEG performance. From this picture, a higher substrate material conductivity can lead to a higher maximum temperature difference on the thermoelectric couple. Based on the working principle of a TEG, the substrate material conductivity has a positive effect on the TEG performance. However, when the conductivity reaches a large value, the temperature difference on the couple is very close to the temperature difference on the whole TEG, which is a fixed value. This is the main reason why the influence of a higher conductivity on the TEG performance is limited.
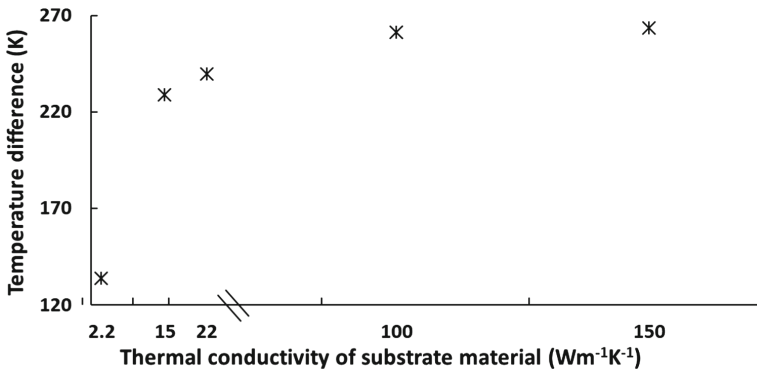
Fig. 15. Maximum temperature gradient of the couple varying with substrate material

6 Conclusions

In this paper, a TEG with constant and variable material properties was simulated with ANSYS-Workbench. The simulation results were validated by experimental results. The results with variable properties were much closer to the experimental data than those with constant properties. The validated TEG model with variable properties led to the following conclusions.

1. Shape factor ratio plays an important role in the TEG performance. It was shown by the modeling study that there is an extremum value in the effect of D on its performance. For this study, the maximum output power and efficiency happened at $D = 1$.
2. The increase of the hot temperature caused an obvious growth in the TEG output power, as it made the TEG work in a higher temperature gradient environment. However, a higher hot temperature is associated with a higher thermal input, having an adverse impact on the TEG efficiency. Therefore, the influence on efficiency is a decrease with a rise of the hot temperature.
3. The couple length also has a significant influence on TEG performance. According to the simulation, there was an opposite effect of the couple length on the output power and efficiency. The increase of the internal resistance, resulting from a longer couple length, is considered as one of the main reasons.
4. Finally, five kinds of substrate materials were analysed in this modeling study. The results indicate that the substrate material with a high thermal conductivity can improve the TEG performance. Nevertheless, the positive effect was not linear because the temperature difference on the thermoelectric couple was very close to the fixed temperature condition for the whole TEG device when the substrate material conductivity arrived at a specific large value.

References

1. Çengel, Y.A., Boles, M.A.: Thermodynamics: An Engineering Approach, 6th edn. McGraw-Hill, New York (2008)
2. Orr, B., Singh, B., Tan, L., et al.: Electricity generation from an exhaust heat recovery system utilizing thermoelectric cells and heat pipes. Appl. Therm. Eng. **73**(1), 588–597 (2014)
3. Twaha, S., Zhun, J., Yan, Y.Y., et al.: A comprehensive review of thermoelectric technology: materials, applications, modelling and performance improvement. Renew. Sustain. Energy Rev. **65**, 698–726 (2016)
4. Chen, M., Gao, J.L., Kang, Z.D., et al.: Design methodology of large-scale thermoelectric generation: a hierarchical modeling approach. J. Therm. Sci. Eng. Appl. **4**(4), 041003-1–041003-9 (2012)
5. He, H.L., Wu, Y., Liu, W.W., et al.: Comprehensive modeling for geometric optimization of a thermoelectric generator module. Energy Convers. Manag. **183**, 645–659 (2019)
6. Siddique, A.R.M., Mahmud, S., Heyst, B.V.: A review of the state of the science on wearable thermoelectric power generators (TEGs) and their existing challenges. Renew. Sustain. Energy Rev. **73**, 730–744 (2017)
7. Zhao, Y.L., Wang, S.X., Ge, M.H.: Performance investigation of an intermediate fluid thermoelectric generator for automobile exhaust waste heat recovery. Appl. Energy **239**, 425–433 (2019)
8. Armstead, J.R., Miers, S.A.: Review of waste heat recovery mechanisms for internal combustion engines. J. Therm. Sci. Eng. Appl. **6**(1), 014001-1–014001-9 (2013)
9. Jiang, T., Su, C.Q., Deng, Y.D., et al.: Integration of research for an exhaust thermoelectric generator and the outer flow field of a car. J. Electron. Mater. **46**(5), 2921–2928 (2016)
10. Frobenius, F., Gaiser, G., Rusche, U., et al.: Thermoelectric generators for the integration into automotive exhaust systems for passenger cars and commercial vehicles. J. Electron. Mater. **45**(3), 1433–1440 (2015)
11. Köysal, Y., Özdemir, A.E., Atalay, T.: Experimental and modeling study on solar system using linear fresnel lens and thermoelectric module. J. Sol. Energy Eng. **140**, 061003-1–061003-11 (2018)
12. Ando Junior, O.H., Maran, A.L.O., Henao, N.C.: A review of the development and applications of thermoelectric microgenerators for energy harvesting. Renew. Sustain. Energy Rev. **91**, 376–393 (2018)
13. Meng, J.H., Zhang, X.X., Wang, X.D.: Multi-objective and multi-parameter optimization of a thermoelectric generator module. Energy **71**, 367–376 (2014)
14. Karri, N.K., Mo, C.: Structural reliability evaluation of thermoelectric generator modules: influence of end conditions, leg geometry, metallization, and processing temperatures. J. Electr. Mater. **47**(10), 6101–6120 (2018)
15. Wang, J., Lia, Y.L., Zhao, C., et al.: An optimization study of structural size of parameterized thermoelectric generator module on performance. Energy Convers. Manag. **160**, 176–181 (2018)
16. Liu, W.S., Jie, Q., Kim, H.S., et al.: Current progress and future challenges in thermoelectric power generation: from materials to devices. Acta Mater. **87**, 357–376 (2015)
17. Chen, L.S., Lee, J.: Effect of pulsed heat power on the thermal and electrical performances of a thermoelectric generator. Appl. Energy **150**, 138–149 (2015)
18. Farahi, N., Prabhudev, S., Bugnet, M., et al.: Effect of silicon carbide nanoparticles on the grain boundary segregation and thermoelectric properties of bismuth doped Mg2Si0.7Ge0.3. J. Electron. Mater. **45**(12), 6052–6058 (2016)

19. Tan, J.F., Ji, K.P., Guo, X.X., et al.: TEG cold side heat transfer analysis for harvesting the exhaust heat energy. Paper presented at the Conference of the ASME International Design Engineering Technical Conferences and Computers and Information in Engineering, Charlotte, North Carolina, 21–24 August 2016

20. Rezania, A., Rosendhl, L.A.: Thermal effect of ceramic substrate on heat distribution in thermoelectric generators. J. Electr. Mater. **41**(6), 1343–1347 (2012)

21. Ming, T.Z., Yang, W., Huang, X.M.: Analytical and numerical investigation on a new compact thermoelectric generator. Energy Convers. Manag. **132**, 261–271 (2017)

22. Hsu, C.T., Huang, G.Y., Chu, H.S., et al.: Experiments and simulations on low-temperature waste heat harvesting system by thermoelectric power generators. Appl. Energy **88**(4), 1291–1297 (2010)

23. Wang, C., He, W., Tong, Y., et al.: Memristive devices with highly repeatable analog states boosted by graphene quantum dots. Small **13**(20), 1603435 (2017)

24. Chen, H., Wang, C., Dai, Y., et al.: In-situ activated polycation as a multifunctional additive for Li-S batteries. Nano Energy **26**, 43–49 (2016)

25. Shourideh, A.H., Ajram, W.B., Lami, J.A., et al.: A comprehensive study of an atmospheric water generator using peltier effect. Therm. Sci. Eng. Prog. **6**, 14–26 (2018)

26. Antonova, E.E., Looman, D.C.: Finite elements for thermoelectric device analysis in ANSYS. Paper presented at ICT 2005, 24th International Conference on Thermoelectrics, Clemson, SC, USA, 19–23 June 2005

27. Sun, H., Ge, Y., Liu, W., et al.: Geometric optimization of two-stage thermoelectric generator using genetic algorithms and thermodynamic analysis. Energy **171**, 37–48 (2019)

28. Khalil, H., Hassan, H.: 3D study of the impact of aspect ratio and tilt angle on the thermoelectric generator power for waste heat recovery from a chimney. J. Power Sources **418**, 98–111 (2019)

29. Fraisse, G., Ramousse, J., Sgorlon, D., et al.: Comparison of different modeling approaches for thermoelectric elements. Energy Convers. Manag. **65**, 351–356 (2012)

30. Electronics Cooling (2019). https://www.electronics-cooling.com/1999/09/the-thermal-conductivity-of-ceramics/. Accessed 10 June 2019